Available online at www.sciencedirect.com
SCIENCE DIRECT®
Surface Science 575 (2005) 233–246
SURFACE SCIENCE
www.elsevier.com/locate/susc

Surface alloys, overlayer and incommensurate structures of Bi on Cu(1 1 1)

D. Kaminski, P. Poodt, E. Aret, N. Radenovic, E. Vlieg *

IMM Department of Solid State Chemistry, Radboud University Nijmegen, Toernooiveld 1, 6525 ED Nijmegen, The Netherlands

Received 20 September 2004; accepted for publication 1 November 2004

Abstract

Using surface X-ray diffraction, we have determined the structure of three different sub-monolayer phases of Bi on Cu(1 1 1). In contrast to an early report, we find that at a coverage of 1/3 monolayer a substitutional surface alloy is formed with a $(\sqrt{3}\times\sqrt{3})R30°$ unit cell. For increasing coverage, de-alloying occurs, leading to an overlayer structure at a coverage of 0.5 ML in which the Bi atoms form zigzag chains. The surface contains three domains of this $\begin{pmatrix} 2 & 0 \\ 1 & 2 \end{pmatrix}$ phase. Finally, at a slightly higher coverage of 0.53 ML, the $\begin{pmatrix} 2 & 0 \\ 1 & 2 \end{pmatrix}$ unit cell is compressed in one direction, leading to a uniaxial-incommensurate phase with three rotational domains.

The structure determination includes relaxations in the topmost layers and therefore allows a detailed comparison of the most important bond distances. This shows that an increased charge density of the Cu(1 1 1) surface is the main driving force for the different phases.

Keywords: X-ray scattering, diffraction and reflection; Surface relaxation and reconstruction; Surface structure, morphology, roughness, and topography; Copper; Bismuth

1. Introduction

The field of metal-on-metal thin films has proved to be interesting and important for both basic and applied science. Many properties arise due to the low-dimensional character of thin films that have no analogue in the bulk. The formation of surface alloys of materials that are normally immiscible is an example that allows the tailoring of surface properties in a novel way. Such surface alloys can be applied in catalysis [1] or in thin film growth where the immiscible species can act as a surfactant [2,3]. The subject of surface alloys has extensively been reviewed recently [4].

* Corresponding author. Tel.: +31 243653070; fax: +31 243653067.
E-mail address: e.vlieg@science.ru.nl (E. Vlieg).

0039-6028/$ - see front matter © 2004 Elsevier B.V. All rights reserved.
doi:10.1016/j.susc.2004.11.001

The best-studied model system of a surface alloy of bulk-immiscible materials is Pb on Cu substrates, where observations have been made on (1 1 1), (1 0 0) and (1 1 0) surfaces [5]. In all cases a random surface alloy is formed at low coverages. On the (1 1 1) and (1 1 0) surfaces, de-alloying occurs for increasing coverages, i.e., the Pb forms an overlayer at such coverages [6]. On the (1 0 0) surface an ordered surface alloy is formed at a coverage of 0.375 monolayer (ML), but also there de-alloying occurs for higher coverages [7]. A similar sequence is found for Bi on Cu(1 0 0), where, as a function of coverage, a disordered surface alloy and a $c(2\times 2)$ ordered surface alloy are formed, followed by de-alloying [8,9]. While this sequence is thus quite common, it does of course not always occur. In the case of Sb on Ag(1 1 1) and Cu(1 1 1), a disordered surface alloy is transformed into a $(\sqrt{3}\times\sqrt{3})R30^\circ$ reconstruction at a coverage of 1/3 ML [10,11]. De-alloying does not occur in this case.

In order to gain more insight into the behaviour of surface alloys, we have studied the Bi–Cu(1 1 1) system. Because surfaces are generally under tensile stress [12], the incorporation of larger atoms is a mechanism to gain surface energy [13]. Bi on Cu thus seems a good candidate for a surface alloy. While Delamare and Rhead state in their pioneering work of 1973 on this system that mixed layers would be improbable [14], we find in fact that at low coverage a genuine surface alloy is formed on the (1 1 1) surface, similar to the (1 0 0) surface. We will refer to the paper of Delamare and Rhead [15] as DR from now on. Starting as a random surface alloy for low Bi coverages, at a coverage of 1/3 ML a well-ordered $(\sqrt{3}\times\sqrt{3})R30^\circ$ reconstruction is formed (called $\sqrt{3}$ from now on). For increasing Bi coverages, de-alloying occurs and a reconstruction is formed with a coverage of 0.5 ML and a unit cell given by $\begin{pmatrix} 2 & 0 \\ 1 & 2 \end{pmatrix}$ in matrix notation. For convenience, we will write this matrix as [2 0 1 2] in the following. Finally, at slightly higher coverage (0.53 ML), an overlayer is formed that is incommensurate in one direction and commensurate in the other (uniaxial-incommensurate). In this paper we present detailed structure determinations of those three phases using surface X-ray diffraction, and discuss the driving forces for their formation.

2. Experimental section

X-ray diffraction is a suitable technique for surface structure determination [16,17]. As a consequence of the 2-dimensional character of the surface, the scattering is diffuse in the direction perpendicular to the surface. These diffraction rods can either originate from the surface super cell in case of a reconstructed surface (fractional-order rods) or can contain contributions from both bulk and surface in so-called crystal truncation rods (integer-order rods). From the intensity distribution along a rod, the surface structure can be derived.

The measurements were performed at the DUBBLE beamline at the European Synchrotron Radiation Facility (ESRF), Grenoble [18]. For all experiments X-rays with an energy of 16 keV ($\lambda = 0.78$ Å) were used. Data from two different experimental runs proved that the results are very reproducible. The set-up consists of an ultra high vacuum (UHV) chamber (pressure $\sim 3\times 10^{-9}$ mbar) coupled to a (2 + 3)-diffractometer operating in a vertical geometry [19,20]. The crystal was mounted in the UHV chamber with the surface normal in the horizontal plane. Bi was deposited from a Knudsen effusion cell at a rate of about 7×10^{-4} ML/s. The deposition rate was initially estimated from the shape of the X-ray intensity during deposition, and was precisely known once we established the coverage of the ordered phases. In order to prepare well-ordered surface phases the substrate temperature was about 315 °C during deposition, but the data acquisition was carried out at room temperature. Most data were collected with a fixed incoming angle of 1°, but in order to increase the measured range of the rods (limited by the Be window of the UHV chamber) we also did measurements with a 15° incoming angle. After applying the necessary correction factors [21], we found the data sets collected for 1° and 15° to give consistent results within the error level of 6%. Note that the correction procedure puts all rods on the same relative scale, except for the specular rod. The atomic posi-

tions in the surface unit cell are fitted to the experimentally determined structure factors using a χ^2 minimization method in the ROD surface crystallography software [22].

The cylindrical Cu(1 1 1) crystal had a diameter of 8 mm and was polished within ~0.3° of the crystallographic (1 1 1) plane [23]. In order to remove the surface damage from the polishing treatment, the sample was annealed to a temperature sufficient for significant sublimation to occur (above 950 °C for 1 h). For cleaning, many cycles of sputtering (600 eV Ar^+ for 15 min at room temperature) and annealing (700 °C for 15 min) were done. Unfortunately the Cu(1 1 1) crystal was found to consist of several grains, which made extended azimuthal scans necessary to obtain accurate structure factors.

We use a (1 1 1) surface unit cell to describe our results. The lattice vectors $\mathbf{a}_i$ are expressed in terms of the conventional cubic lattice vectors by

$$\mathbf{a}_1 = \frac{1}{2}[1\,0\,\bar{1}]_{\text{cubic}}, \quad \mathbf{a}_2 = \frac{1}{2}[\bar{1}\,1\,0]_{\text{cubic}},$$
$$\mathbf{a}_3 = [1\,1\,1]_{\text{cubic}}$$

with

$$|\mathbf{a}_1| = |\mathbf{a}_2| = \frac{1}{2}\sqrt{2}a, \quad |\mathbf{a}_3| = \sqrt{3}a,$$

and where a is the lattice constant of Cu (3.61 Å). The corresponding reciprocal lattice vectors $\mathbf{b}_j$ are defined by $\mathbf{a}_i \cdot \mathbf{b}_j = 2\pi\delta_{ij}$. The momentum transfer vector is then given by $\mathbf{Q} = h\mathbf{b}_1 + k\mathbf{b}_2 + l\mathbf{b}_3$ with (hkl) the diffraction indices. With our (conventional) choice of the surface unit cell the index l is along the direction perpendicular to the surface. Crystal truncation rods have integer (hk) indices, the extra rods from the surface reconstructions have fractional (hk) indices.

3. Results

By choosing a sensitive reflection, the growth of the Bi layer can be followed precisely during deposition [24]. A typical deposition curve is shown in Fig. 1a, where the intensity of the (0 0 1.9) reflection is plotted as a function of time. Overall, we find good agreement with the results and the phase diagram proposed by DR. The solid vertical lines in Fig. 1 labeled 1/3 and 1/2 ML correspond to the ideal coverages for the $\sqrt{3}$ and the [2 0 1 2] phases. The break in between these points (near 0.43 ML) marks the end of the coexistence regime of the two phases, as will be discussed in more detail later. Finally at a coverage of 0.53 ML the entire surface is covered by an incommensurate structure.

The $\sqrt{3}$ phase is called structure I by DR, the [2 0 1 2] phase structure II. Note that due to a non-conventional choice for the surface unit cell, the [2 0 1 2] phase is written as [2 0 2 $\bar{1}$] by DR. From the X-ray diffraction, we determined that at a coverage of 0.53 ML an incommensurate phase occurs. DR also reported a third phase ("structure III"), but claimed this to be a $(\sqrt{7}\times\sqrt{7})19°$ phase. This will be discussed in more detail below.

Additional deposition curves using different temperatures and observing different reflections all agreed with the phase diagram in Fig. 1. Reflection high-energy electron diffraction (RHEED) was performed as well and again confirmed the phase behaviour. The deposition profile of the (0 0 1.9) reflection shows that above 0.53 ML the intensity stays constant. This indicates that the surface structure does not change any more and that the extras Bi atoms form 3D islands on the surface.

3.1. The $(\sqrt{3}\times\sqrt{3})R30°$ phase

This phase was prepared by deposition of 1/3 ML Bi with the substrate at 315 °C. After that the crystal was cooled down to room temperature. In this way a well-ordered $\sqrt{3}$ phase is formed, with a coherence length of $L = 2/\Delta q_{\text{fwhm}} \approx 900$ Å as estimated from the peak width of the fractional-order peaks [25]. For the $\sqrt{3}$ phase, the (1 0), (1 1) and (0 0) rods as well as the (1/3, 4/3) and (2/3, 5/3) fractional rods were measured (see Figs. 2 and 3). The negative values of l were obtained by inverting the structure factors through the origin of reciprocal space (Friedel's rule). In addition, a full in-plane data set was obtained at $l = 0.3$. Since the scattering cross sections of Cu ($Z = 29$) and Bi ($Z = 83$) are quite different, the fractional-order reflections are easily observable.

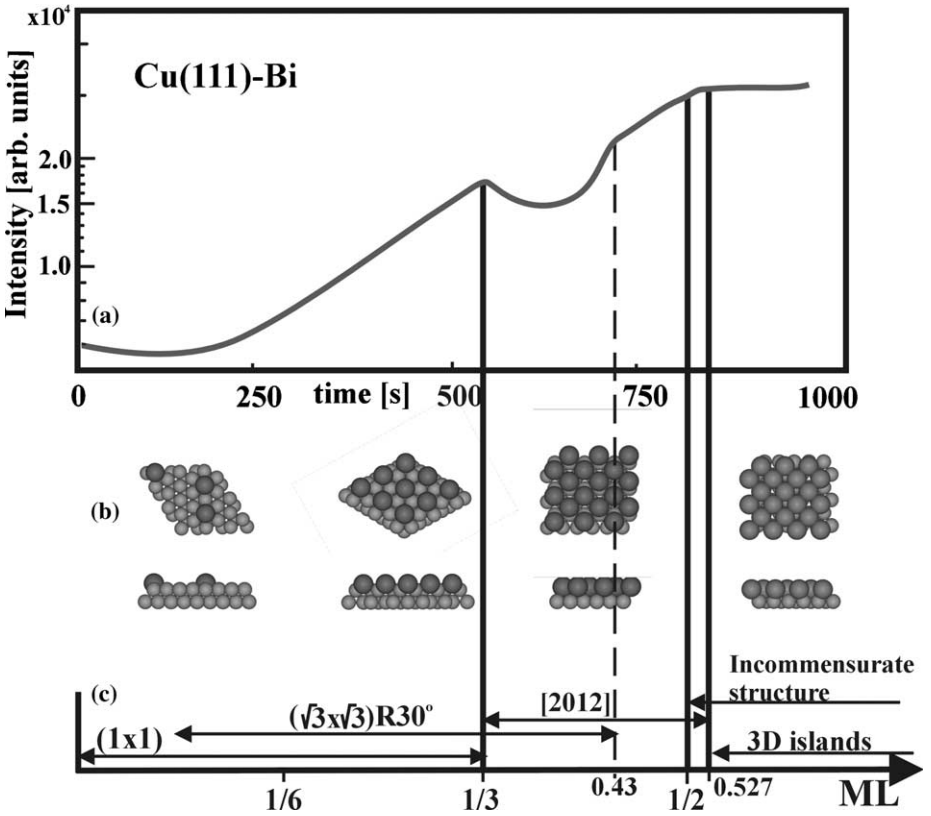

Fig. 1. (a) The (0 0 1.9) reflection during Bi deposition at a Cu(1 1 1) substrate temperature of 315 °C, (b) miniatures of the four different surface structures and (c) a room temperature phase diagram showing the coverage over which the various surface phases occur.

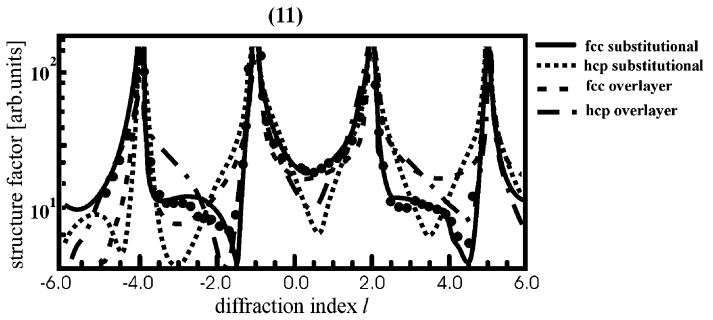

Fig. 2. Structure factor amplitudes $|F_{hkl}|$ along the (1 1) rod measured on Cu(1 1 1)–$(\sqrt{3}\times\sqrt{3})R30°$-Bi. The measured structure factors are indicated by filled circles. Calculations are shown for four models: with normal (fcc) or faulted (hcp) stacking, and with Bi at substitutional or overlayer sites.

The data on the $\sqrt{3}$ phase were measured after those of the [2 0 1 2] phase. The systematic error between equivalent reflections for this sample and geometry was therefore known to be ~6% and only a limited amount of equivalent reflections were measured on the $\sqrt{3}$ phase. The total data set consisted of 168 reflections, with 146 non-equivalent ones.

Establishing the correct structure model is straightforward for the $\sqrt{3}$ reconstruction, because

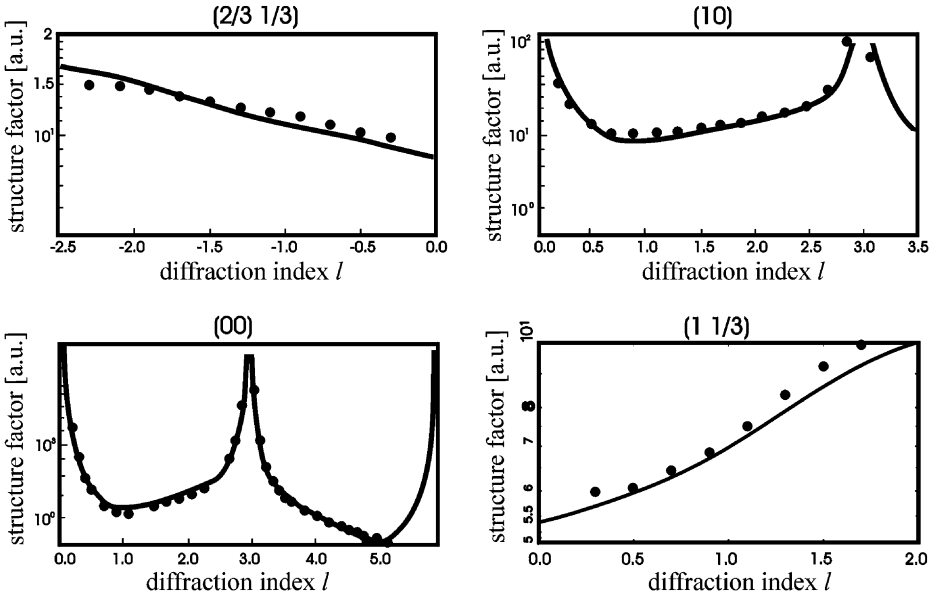

Fig. 3. Structure factor amplitudes $|F_{hkl}|$ along the (2/3, 1/3), (1 0), (0 0) and (1, 1/3) rods measured on Cu(1 1 1)–$(\sqrt{3}\times\sqrt{3})R30°$-Bi. Measured structure factors are indicated by filled circles. The solid curves represent calculations for our best-fit model.

this type has been found in other systems as well, like Pb–Cu(1 1 1) [26], Pb–Ni(1 1 1) [27,28] and Sb–Ag(1 1 1) [11]. From the deposition curves, the coverage is estimated to be around 0.3 ML, corresponding to the expected value of 1 Bi atom per $\sqrt{3}$ cell. Four simple models are then possible: Bi at a substitutional or an overlayer site and for each a normal fcc or a faulted hcp stacking. As shown in Fig. 2, calculations based on these models immediately rule out the overlayer and stacking fault models, leaving the substitutional surface alloy as only possibility.

In order to get a proper fit, relaxation of the surface atoms has to be taken into account. Fig. 4 shows the structural model together with the symmetry-allowed relaxations. Especially an out-of-plane relaxation for Bi significantly improved our model; this is as expected because the Bi atomic radius is larger than that of Cu. Other relaxations were small and only relaxation in the two topmost layers were required. For example the relaxation in second layer $\Delta z_{Cu2} = 0.01 \pm 0.01$ Å is already at the detection limit. Additional fitting parameters are enhanced Debye–Waller para-

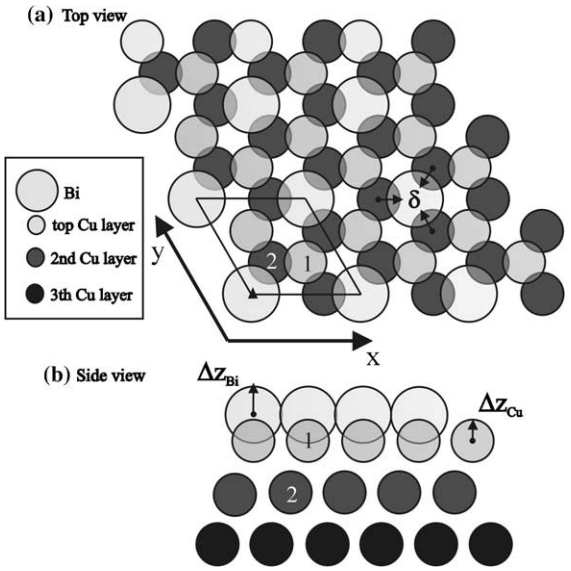

Fig. 4. Schematic of our structural model for the Cu(1 1 1)–$(\sqrt{3}\times\sqrt{3})R30°$-Bi reconstruction, with the unit cell indicated in (a). Non-equivalent surface atoms are labeled by different numbers. Arrows indicate the allowed relaxation directions in our fitting procedure. The nearest-neighbor distances derived from our best-fit model are listed in Table 1.

Table 1
Structure parameters for the best-fit model of Cu(111)–$(\sqrt{3}\times\sqrt{3})R30°$-Bi

Fit parameter	Value
Δz_{Bi} (Å)	1.02(2)
Δz_{Cu1} (Å)	0.03(1)
Δz_{Cu2} (Å)	0.01(1)
δ (Å)	0.008(6)
DW_{Cu1} (Å^2)	1.4(1)
$DW_{\parallel,Bi}$ (Å^2)	2.7(1)
$DW_{\perp,Bi}$ (Å^2)	0.8(1)
χ^2	2.01
Inter atomic distances (Å)	
Bi–Cu_1	2.76
Bi–Cu_2	3.48
Cu_1–Cu_2	2.58

Deeper layers are fixed at bulk positions. The DW parameter for the bulk atoms is fixed at 0.51. The displacements are with respect to a bulk-terminated substrate.

meters for the topmost layer, where the Bi atoms have anisotropic thermal vibration amplitudes. By testing models with different sets of fitting parameters, we found that we could obtain optimum results using these parameters, together with a global scale factor and a separate scale factor for the specular rod. Our best-fit model has a reduced χ^2 of 2.01, the corresponding fit parameters are listed in Table 1 and the fits are shown in Fig. 3. When preparing the $\sqrt{3}$ phase, we deposited slightly more than 1/3 ML Bi. The surface therefore contains a small fraction with the [2 0 1 2] phase, which leads to a slightly worse fit.

The height difference between the bismuth and copper atoms in the surface layer is found to be 0.99 Å. This means that Bi atoms stick significantly out of the last Cu layer.

3.2. The [2 0 1 2] phase

The [2 0 1 2] phase was prepared by depositing 0.5 ML Bi at 315 °C. At this temperature the [2 0 1 2] structure is in fact molten [29], the reconstruction is formed by cooling below 240 °C. The first data were collected at 50 °C with the sample still cooling down, but most of the data were obtained at 25 °C. The measured reflections of the surface reconstruction are all 1/4 order, suggesting a 4×4 unit cell. There are, however, many systematic absences and the correct surface unit cell is given by the matrix [2 0 1 2] as already determined by DR [15]. The in-plane lattice vectors have lengths of 5.11 Å and 4.42 Å, with a 90° angle. The P3 symmetry of the substrate leads to three equivalent [2 0 1 2] domains, which yields the (incomplete) 1/4 order reciprocal space.

We measured data for all three domains. By an appropriate coordinate transformation, the data of domains 2 and 3 were mapped on that of domain 1. We further found a single domain to have Pm symmetry. Using these symmetries, the total of 312 measured reflections were reduced to 196 non-equivalent ones, consisting of the (0 0), (1 0), (1 1) and (2 0) integer-order rods, the (0.5, 0.25) and (0.5, 0.75) fractional-order rods, and an in-plane data set. The average agreement factor was 6%. Part of the data is shown in Fig. 5. From the width of fractional peaks, a correlation length of 850 Å was calculated.

From the deposition curve a Bi coverage of 0.5 ML is estimated, corresponding to two Bi atoms per unit cell. This again agrees with DR. DR did not perform a quantitative structure analysis, but proposed a simple overlayer model with one Bi atom at the origin and the other at the centre of the surface unit cell. The Patterson map calculated from the in-plane fractional-order data shows that this is indeed a nearly correct model (see Fig. 6). However, the ellipsoidal shape of the central contour indicates some lateral relaxations. From the fit we find that the Bi atoms relax laterally such that they occupy positions closer to threefold hollow sites. The nearly constant amplitude along the fractional-order rods (see Fig. 5) shows that the reconstruction is mainly confined to a single layer. We indeed find, by trying various models and different degrees of freedom, that the parameters describing the Bi atoms are the most important. The fitting parameters used are thus: lateral relaxations along the y-direction (in agreement with the Pm symmetry), perpendicular relaxation and anisotropic DW parameters (see Fig. 7). The two Bi atoms are not on symmetry-related sites, thus their parameters need not be the same. From the fit to the data, we nevertheless found the parameter values of the two atoms the be so similar that using the same value for both yields

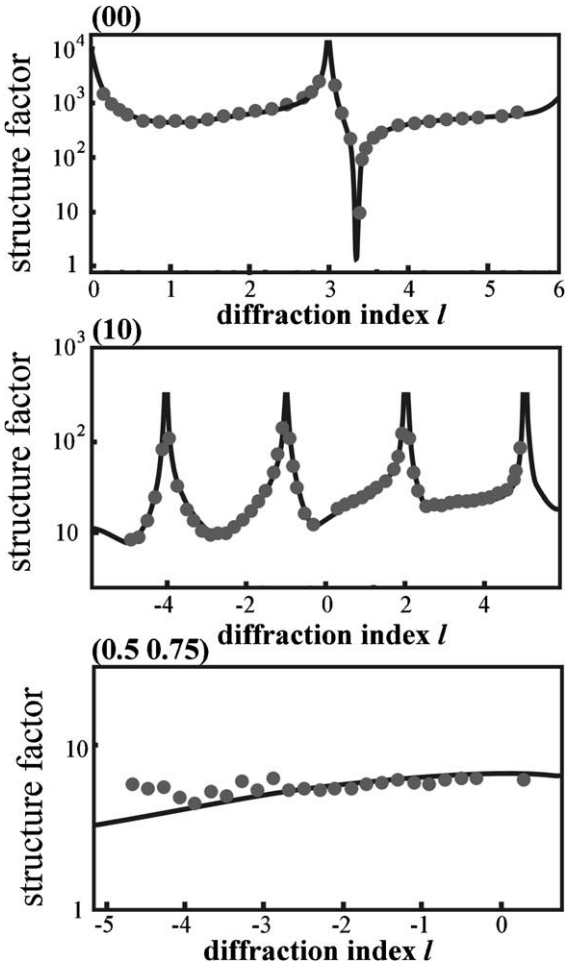

Fig. 5. Structure factor amplitudes along the (0 0), (1 1) and (0.5, 0.25) rods for the [2 0 1 2] reconstruction of Bi on Cu(1 1 1). Circles indicate data, the solid curves represent the best-fit model.

a fit with essentially the same quality. Rather then using a centred unit cell for the starting position of the Bi atoms, we use the two hollow sites shown in Fig. 7 as a start. We then find that the Bi atoms symmetrically move away in order to increase their mutual distance from 2.95 to 3.20 Å. Perpendicular relaxation of the topmost Cu layer was smaller then the resolution of our data for all three non-equivalent Cu atoms, as expected from the fractional-order rods. Also roughness was found to be negligible. With these parameters (and two scale factors) we find an excellent fit to the data (see Fig. 5) with a χ^2 value of 1.89. The best fit parameters

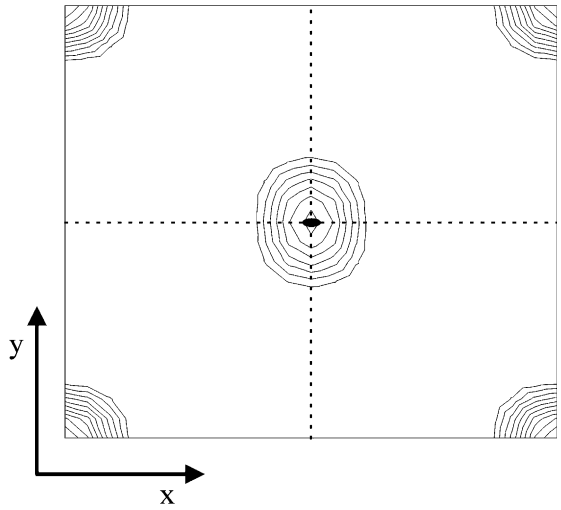

Fig. 6. Surface projected Patterson map generated from the in-plane fractional order reflections shows only two peaks corresponding to two Bi atoms per unit cell. The ellipsoidal contour in the middle indicates that the central Bi atom is not precisely in the middle of the unit cell.

are listed in Table 2. We thus find the Bi atoms to be located close to the threefold hollow sites of the substrate, forming zigzag chains. At the data acquisition temperature of 25° C, the Bi atoms have an enhanced in-plane thermal vibration amplitude. If the occupancy of the Bi atoms is added as fitting parameter, we obtain a slightly improved fit ($\chi^2 = 1.74$) with an optimum value for the occupancy of 0.92, but all the other fitting parameters are the same within the error bars. Some of the Bi positions may thus be empty or occupied by Cu atoms.

3.3. Uniaxial incommensurate surface phase

The incommensurate phase was prepared by depositing approximately 1 ML Bi with the substrate at 280 °C. This is above the ideal coverage, but the excess is used to compensate for the desorption that takes place at the preparation temperature. At 280 °C the Bi layer is molten, but the structure is formed by cooling below 240 °C. All data were collected at 25 °C.

The deposition curve in Fig. 1 (and similar curves measured under various other conditions) indicate the existence of a surface phase with a

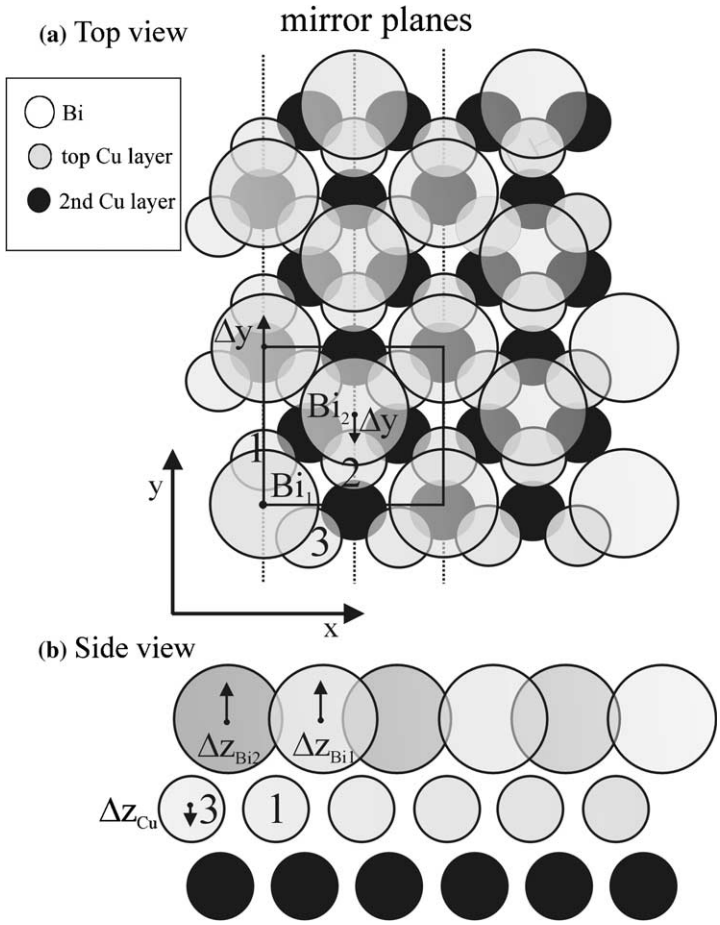

Fig. 7. Schematic of the model for the [2 0 1 2] reconstruction, with the unit cell indicated. Arrows indicate the allowed relaxation directions in our fitting procedure, their values are given in Table 2.

coverage near 0.53 ML (as derived with respect to the ideal coverage of the [2 0 1 2] phase). DR proposed that this was a $(\sqrt{7}\times\sqrt{7})R19.1^\circ$ phase, but this turns out not to be the case for our preparation conditions. First of all, such a unit cell would give ideal coverages in multiples of 1/7, but the closest match of 4/7 = 0.57 ML still disagrees with the observed 0.53 ML. The size of the surface unit cell can more precisely be determined from the diffraction indices corresponding to the reconstructed unit cell. We determined the diffraction indices of one of the reflections to be (0.527, 0.235) (with an error of ±0.001). This does not correspond to any $(\sqrt{7}\times\sqrt{7})R19.1^\circ$ reflection, only the (4/7, 1/7) = (0.571, 0.286) is relatively close and probably explains the erroneous assignment of DR.

By measuring several surface reflections, we determined that the surface phase consists of three domains, each of which is commensurate in one and incommensurate in the other direction (see Fig. 8). For this uniaxial-incommensurate phase a primitive unit cell can be defined, but we will use here a more convenient (and conventional) centred rectangular cell. The lattice parameters of this cell can be calculated from the observed surface reflections to be $a_{1,ic} = 4.848$ Å and $a_{2,ic} = 4.431$ Å. Comparing this to the lattice parameters of the [2 0 1 2] unit cell of 5.112 Å and 4.427 Å respectively, we find that the lattice is commensurate with the substrate along the $\mathbf{a}_{2,ic}$ direction (same lattice parameter within the error bar of the measurement), but that along the $\mathbf{a}_{1,ic}$ direction

Table 2
Structure parameters for the best-fit model of the Cu(1 1 1) [2 0 1 2]-Bi surface reconstruction and the atom distances near the surface

Fit parameter	Values
$\Delta z_{Bi1,Bi2}$ (Å)	0.35(1)
$\Delta z_{Cu1,2,3}$ (Å)	−0.01(3)
Δy (Å)	0.13(1)
$DW_{\parallel,Bi1,Bi2}$ (Å^2)	3.8(2)
$DW_{\perp,Bi1,Bi2}$ (Å^2)	1.4(3)
χ^2	1.89
Inter atomic distances (Å)	
Bi_1–Bi_2	3.57
Bi_1–Bi_2	3.20
Bi_1–Cu_1	2.75
Bi_1–Cu_2	3.76
Bi_1–Cu_3	2.93
Bi_2–Cu_1	3.76
Bi_2–Cu_2	2.75
Bi_2–Cu_3	2.93

Deeper layers are fixed at bulk positions. DW parameters for the Cu atoms are fixed at the bulk value of 0.51. The relaxations of the Bi atoms are with respect to bulk-extrapolated, hollow sites.

the new unit cell is 5.2% smaller and is incommensurate. With two atoms per incommensurate unit cell (because it is a centred lattice), the ideal coverage of the incommensurate phase is given by the ratio of the a_1 lattice parameters, leading to an ideal coverage of $0.5 \times (5.112/4.848) = 0.527$ ML, in perfect agreement with the 0.53 ML estimated from the deposition curves.

We measured in-plane and rod data for all three domains, with a total of 101 reflections. Fig. 9 shows a part of our data set: the (0 0), (1 1) integer rods and the (0.527, 0.235) incommensurate rod. The average agreement factor between equivalent reflections was 6%. A fully incommensurate phase would not contribute to the substrate rods except for the specular rod. In our case, however, one direction is commensurate and the Fourier components along that direction contribute to the corresponding substrate rods. With respect to the substrate unit cell, the Bi atoms occupy all possible positions in the incommensurate direction, and can thus be viewed as a continuous row of charge distribution. For non-specular reflections, at maximum one of the three equivalent domains will contribute to a substrate rod. This is sufficient to determine the registry of the incommensurate unit cell with respect to the substrate (i.e., the height and the lateral position in the commensurate direction) and the Debye–Waller parameter of the Bi atoms. There are no other structural parameters, because the Bi overlayer contains only one unique atom per centred asymmetric unit. In order to perform the actual fit, we simply used the [2 0 1 2] surface unit cell, but now with the second Bi atom exactly centred with respect to the first one. Since the ideal coverage for the incommensurate phase is 0.527 ML, the occupancy of each atom is expected to be 0.527/0.5 = 1.054. The continuous row of charge distribution along the incommensurate direction is approximated by generating a row of five, equally-spaced Bi atoms in this direction. With this trick only the commensurate direction contributes to the rods measured here. Using this model, we obtained excellent fits (see Fig. 9). The best fit parameters are listed in Table 3.

As in the case of the [2 0 1 2] structure, roughness was found to be negligible. The measured height of the Bi atoms above the top most Cu layer is the same as in case of the [2 0 1 2] structure. However, the registry of Bi in the y-direction is different, because the incommensurate surface unit cell is centred. We can estimate the y-position based on symmetry. The two atoms should have the same position with respect to the underlying Cu rows, thus Δy with respect to the hollow site (see Fig. 7) should be the same. This leads to y-positions in fractional coordinates of $1 + \Delta y$ and $2/3 - \Delta y$ for atom 1 and 2 respectively. At the same time, the unit cell is centred, meaning that the difference in y should be 0.5. This yields $\Delta y = 1/12$ or 0.37 Å. This displacement puts the Bi atoms in the centre of the Cu rows, a position one would expect from symmetry.

The fitted value $\Delta y = 0.39(3)$ Å is indeed within error the expected value. The smooth profile of the (0.527, 0.235) incommensurate rod (Fig. 9) excellently fits to the simple surface model with a single layer of Bi without bulk contribution. For the best fit $\chi^2 = 4.1$. From the figures, the fit quality appears to be the same as for the other structures; the higher χ^2 is probably due to an underestimation of the errors in the data. Similarly to the situation for the [2 0 1 2] structure, if the occupancy of the Bi atoms is added as a fitting parameter, the fit

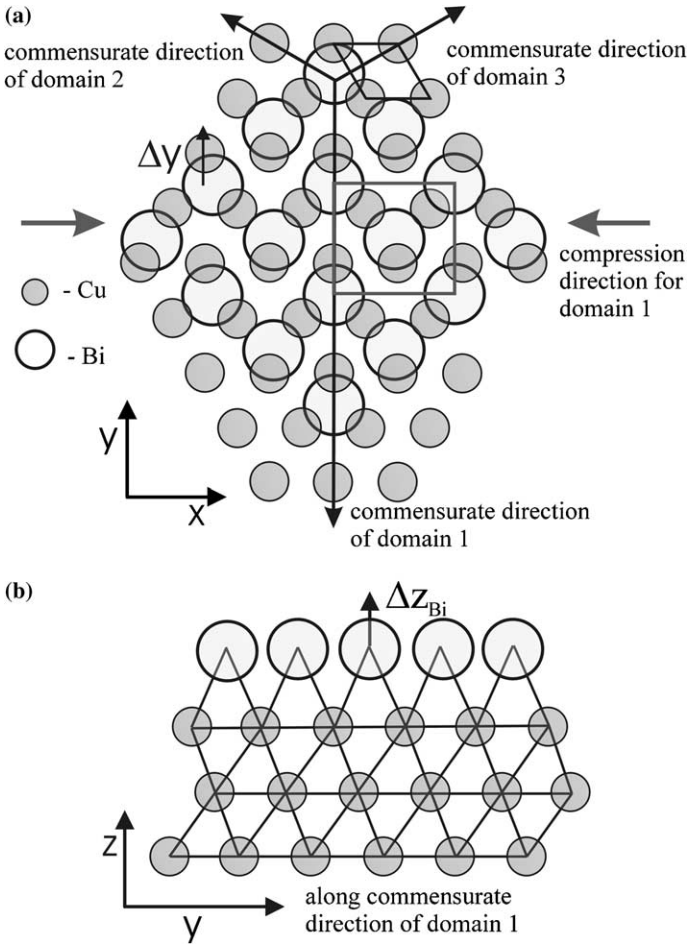

Fig. 8. (a) The three domains of the uniaxially-incommensurate structure as caused by the P3 symmetry of the substrate. The commensurate directions are indicate by black arrows. The Cu surface unit cell is shown on top. (b) Side view along the commensurate direction. The Bi atoms are positioned in the middle of the two underlying Cu rows. The two fitted displacement parameters are indicated as well; Δy is measured with respect to a threefold hollow site.

is slightly improved ($\chi^2 = 3.4$) with an optimum occupancy value of 0.89(5), but all the others fitting parameters are the same within the error bars, see Table 3. The reason for this apparent lower occupancy is not clear, in particular since the surface has an excess of Bi in 3D islands.

3.4. Low coverage phase

At very low coverage there is a fourth phase for which we obtained only limited data. From deposition curves (e.g. Fig. 1), we conclude that the structure factors vary smoothly until the appearance of the $\sqrt{3}$ phase, proving that the Bi atoms have the same substitutional site as in that phase. RHEED experiments show that the $\sqrt{3}$ phase only starts forming for coverage above 0.13 ML. We may thus conclude that for a Bi coverage below 0.13 ML, the Bi atoms are located at substitutional sites and are disordered, i.e., they form a lattice gas.

4. Discussion

Having established the atomic structures of four phases, we can now discuss the physics behind the

behaviour as a function of coverage. From the perspective of the clean Cu(1 1 1) substrate, the main driving force is to increase the coordination of the surface layer. The reduced density at the surface leads to a tensile stress [12] that can be lifted by incorporating larger atoms [13], i.e., Bi in the case studied here. We have found that at low coverages, the Bi atoms indeed occupy substitutional sites in the topmost layer. The Bi atoms are disordered at low coverages, but above 0.13 ML the lattice gas orders into a $\sqrt{3}$ phase in which the Bi atoms remain at substitutional sites (the onset was determined from RHEED observations). When the Bi coverage reaches 1/3 ML, the entire surface is covered by the $\sqrt{3}$ phase. The transition from a disordered lattice gas into an ordered $\sqrt{3}$ surface alloy has also been observed e.g. Sb on Cu(1 1 1) and Ag(1 1 1) [11]. In that case, the ordering occurred only at a much higher coverage of 0.3 ML, close to the value predicted from the hard-hexagon model in statistical mechanics [30]. From the fact that for the Bi–Cu(1 1 1) system the ordering occurs already at a much lower coverage, we conclude that there is a significant Bi–Bi interaction. The $\sqrt{3}$ phase is similar to that of Pb on Ni(1 1 1) [27,28] because the top layer has a normal fcc stacking, unlike the case of Sb on Cu(1 1 1) and Ag(1 1 1) [11].

Because of the reduction of the tensile surface stress, one expects the Bi to be embedded deeper into the surface than based on a hard sphere model, i.e., one expects a reduced surface rumpling [13]. Using atomic radii for Bi and Cu of 1.63 Å and 1.28 Å respectively, the calculated rumpling is 1.38 Å. The experimental value of 0.99 Å is indeed less than this. As has been observed for several other surface alloys [13], the experimental Bi–Cu bond distance of 2.76 Å is between the values based on atomic radii (2.91 Å) and covalent radii (2.63 Å).

When the Bi coverage exceeds 1/3 ML, it is not favourable to incorporate the extra Bi atoms in the surface layer. Instead, an overlayer with a [2 0 1 2] unit cell is formed. Such an overlayer is an alternative means to provide the extra charge density for the substrate. The Bi–Cu bond distance is 2.75 Å for Cu atoms 1 and 2 (see Fig. 7), very close to the value found in the $\sqrt{3}$ structure. Cu atom 3 has two Bi bonds, which are thus expected to be somewhat longer, as confirmed by the experimental value of 2.93 Å. The bonding of the Bi atoms to the substrate is not enough to reach a fully stable structure, the Bi–Bi interactions are crucial as well. Because of their size, two Bi atoms do not fit in adjacent threefold hollow sites, but are slightly displaced from these positions. This leads to two Bi–Bi bonds with a length of 3.20 Å (plus two longer 'bonds' of 3.57 Å) and gives a chain-like structure of the Bi structure (see Fig. 7).

Our experiments show that the formation of the [2 0 1 2] phase is more favourable than a combination of the $\sqrt{3}$ phase with 3D Bi islands. The ideal coverage of the [2 0 1 2] phase is 0.5 ML, but we find this phase to be already stable at 0.43 ML. As seen by the break in the deposition curve in Fig. 1 (and as confirmed by additional RHEED data), at that coverage there is no longer a coexistence with the $\sqrt{3}$ phase.

When the Bi coverage is increased even further, the balance between Cu–Bi and Bi–Bi interactions in the [2 0 1 2] phase is changed in favour of the Bi–Bi interactions. Now an incommensurate phase is formed (i.e., Bi adopts its own lattice constant), in which each Bi atom has four identical bonds with Bi neighbors and with a length of 3.28 Å. This is slightly longer than in the [2 0 1 2] phase, as expected because of the higher coordination. Of course the bonding to the Cu substrate is still important (in one direction the structure is still commensurate), but now occurs through the average charge density. Similar structures are described in [31,32].

The ideal coverage of the incommensurate phase is 0.527 ML. Between this value and 0.5 ML we find coexistence of the [2 0 1 2] and the incommensurate phase (see Fig. 11). This agrees with the observations of DR (even though they did not identify the incommensurate phase). One can view the formation of the incommensurate phase as a compression of the [2 0 1 2] phase in the x-direction due to the insertion of extra Bi rows, see Fig. 10. This commensurate–incommensurate transition could have followed the Frenkel and Kontorova model [33,34], in which commensurate regions are separated by localized domains of higher density (solitions) [9]. We did, however,

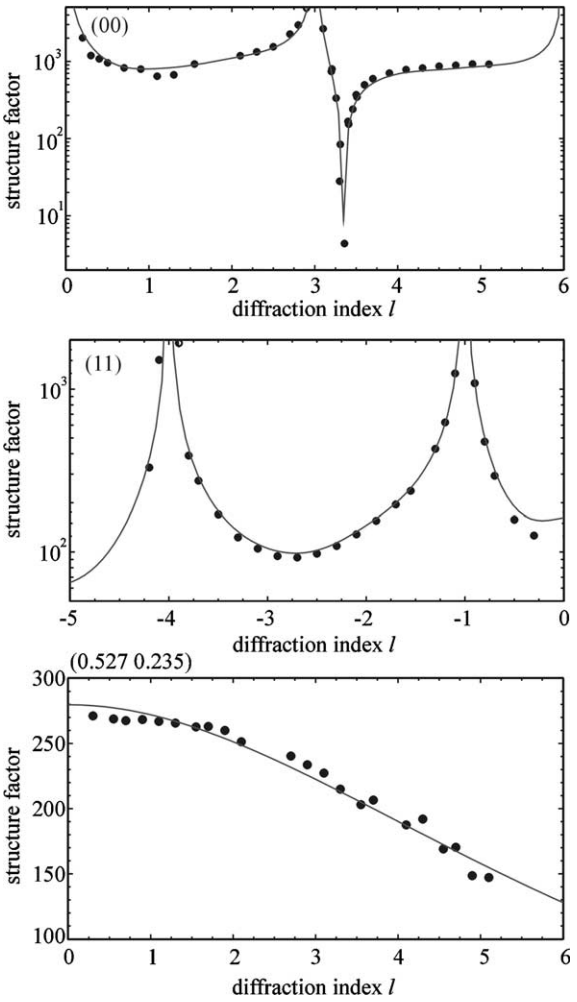

Fig. 9. Structure-factors amplitudes along the (00), (11) and (0.527, 0.235) rods for the incommensurate structure of Bi on Cu(111). Circles indicate measured structure factors, the solid curves represent the best-fit model.

Table 3
Structure parameters for the best-fit model of the Cu(111)—incommensurate surface reconstruction

Fit parameter	Value	Value
Δz_{Bi} (Å)	0.36(2)	0.36(2)
Δy (Å)	0.39(3)	0.40(3)
DW_{Bi} (Å^2)	2.0(4)	1.7(5)
Occupancy	≡1.056	0.89(5)
χ^2	4.1	3.4
Inter atomic distances (Å)		
Bi–Bi	3.28	3.28

All Cu layers are fixed at bulk positions. DW parameters for bulk Cu atoms are fixed at 0.5.

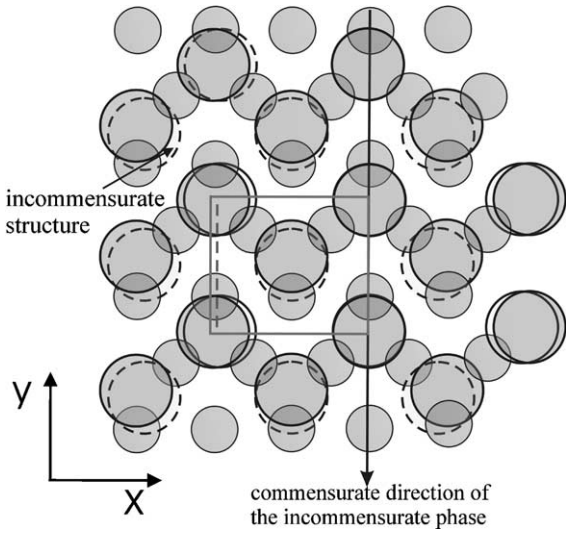

Fig. 10. The [2 0 1 2] and incommensurate structures together. The smaller, dashed frame in the centre indicates the incommensurate unit cell, the larger one the [2 0 1 2] cell. The small circles are the substrate Cu atoms, the large ones the Bi atoms, which are drawn solid and dashed for the commensurate and incommensurate phase, respectively.

not find the continuous change in the position of the diffraction peaks that is expected in this model, but have found coexistence of two phases instead, which indicates well defined domains of the incommensurate phase.

The incommensurate phase is the phase with the highest coverage we have observed. For higher Bi coverages, 3D islands are formed. Overall, the phase behaviour as a function of coverage closely agrees with the results of DR. The behaviour of Bi on the Cu(1 1 1) surface is similar to that on the Cu(1 0 0) surface, where also a surface alloy at low coverage is followed by de-alloying, leading to several overlayer structures [35,36]. From the present data, the kinetic pathways of the various phase transitions as a function of coverage cannot be derived [37], but this has been studied in recent LEEM experiments [38]. Using XRD we have investigated the high-temperature behaviour of the Cu(1 1 1)–Bi system as well [29].

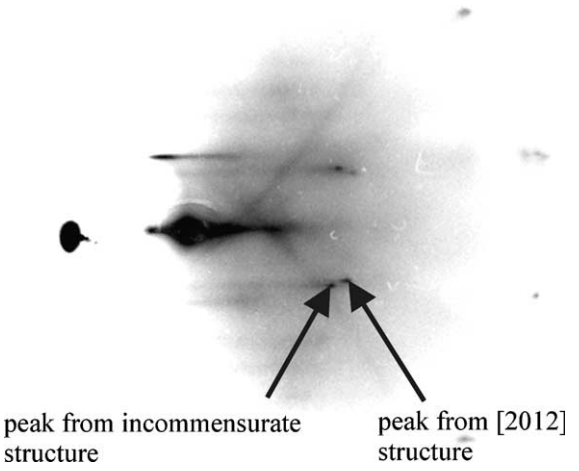

Fig. 11. RHEED picture of the coexistence of the [2 0 1 2] and the incommensurate structure. Black arrows indicate two peaks representing these two structures. The picture was obtained with the substrate at 240 °C with an electron energy of 16 keV.

5. Conclusions

In this paper we have presented the room temperature phase diagram of Bi on Cu(1 1 1) and have solved the structure of three specific surface phases in detail. Bi–Cu(1 1 1) presents a clear case of surface alloying (in the $\sqrt{3}$ phase) followed by de-alloying (the [2 0 1 2] phase) as a function of Bi coverage. The driving force is the tendency of the bare Cu(1 1 1) surface to increase its coordination, by either incorporating the larger Bi atoms (with the expected reduced rumpling), or by the formation of a Bi overlayer.

At a slightly higher coverage, an overlayer phase is formed which is uniaxially incommensurate. For that phase, the Bi–Bi bond in the overlayer appears crucial for the stability. While they thought surface alloying to be unlikely, the symmetry of the $\sqrt{3}$ and the [2 0 1 2] phases agrees with the earlier LEED results by Delamare and Rhead.

Acknowledgments

We thank R. Koper from Surface Preparation Lab. for providing a Cu(1 1 1) crystal at very short notice. We thank the DUBBLE staff for assistance during the experiment, W. Szweryn for technical support and H. Lemmens and Ch. Creusen for detailed RHEED analysis. This work was made possible by financial support from the Council for Chemical Science of the Netherlands Organization for Scientific Research (CW-NWO).

References

[1] F. Besenbacher, B.S.I. Chorkendorff, B. Hammer Clausen, A. Molenbroek, J.K. Norskov, I. Stensgaard, Science 279 (1998) 1013.
[2] H.A. van der Vegt, H.M. van Pinxteren, M. Lohmeier, E. Vlieg, J.M.C. Thornton, Phys. Rev. Lett. 68 (1992) 3335.
[3] J. Camarero, L. Spendeler, G. Schmidt, Phys. Rev. Lett. 18 (1994) 2448.
[4] D.P. Woodruff (Ed.), Surface Alloys and Alloy Surfaces, Elsevier Science B.V., Amsterdam, 2002.
[5] Kellogg, G.K., in: D.P. Woodruff (Ed.), Surface Alloys and Alloy Surfaces, vol. 10, Elsevier, Amsterdam, 2002, p. 152.
[6] C. Nagl, O. Haller, E. Platzgummer, M. Schmid, P. Varga, Surf. Sci. 321 (1994) 237.
[7] C. Nagl, E. Platzgummer, O. Haller, Surf. Sci. 333 (1995) 831.
[8] H.L. Meyerheim, H. Zajonz, W. Moritz, I.K. Robinson, Surf. Sci. 381 (1997) L551.
[9] H.L. Meyerheim, M. De Santis, W. Moritz, I.K. Robinson, Surf. Sci. 418 (1998) 295.
[10] H.A. van der Vegt, J. Vrijmoeth, R.J. Behm, E. Vlieg, Phys. Rev. B 57 (1998) 4127.
[11] S.A. de Vries, W.J. Huisman, P. Goedtkindt, M.J. Zwanenburg, D.S.L. Bennet, I.K. Robinson, E. Vlieg, Surf. Sci. 414 (1998) 159.
[12] H. Ibach, Surf. Sci. Rep. 29 (1997) 195.
[13] D.P. Woodruff, E. Vlieg, in: D.P. Woodruff (Ed.), Surface Alloys and Alloy Surfaces, vol. 10, Elsevier, Amsterdam, 2002, p. 277.
[14] G.F. Rhead, F. Delamare, Surf. Sci. 35 (1973) 172.
[15] G.F. Rhead, F. Delamare, Surf. Sci. 35 (1973) 185.
[16] R. Feidenhans'l, Surf. Sci. Rep. 10 (1989) 105.
[17] I.K. Robinson, D.J. Tweet, Rep. Prog. Phys. 55 (1992).
[18] M. Borsboom, et al., J. Synchrotron Radiat. 5 (1998) 518.
[19] E. Vlieg, A. van't Ent, A.P. de Jongh, H. Neerings, J.F. van der Veen, Nucl. Instr. Meth. A 262 (1987) 522.
[20] E. Vlieg, J. Appl. Cryst. 31 (1998) 198.
[21] E. Vlieg, J. Appl. Cryst. 30 (1997) 532.
[22] E. Vlieg, J. Appl. Cryst. 33 (2000) 401.
[23] Surface Preparation Laboratory, R.J.I.M. Koper, http://www.surface-prep-lab.com.
[24] E. Vlieg, Surf. Sci. 500 (2002) 458.
[25] E. Vlieg, J.F. van der Veen, S.J. Gurman, C. Norris, J.E. Macdonald, Surf. Sci. 210 (1989) 301.

[26] O. Haller, C. Nagi, E. Platzgummer, M. Shmid, P. Varga, Surf. Sci. 321 (1994) 237.
[27] A. Nakanishi, K. Umezawa, T. Yumura, W.M. Gibson, M. Watanabe, Y. Kido, S. Yamamoto, A. Aoki, H. Naramoto, Phys. Rev. B 56 (1997) 10585.
[28] D. Brown, P.D. Quinn, D.P. Woodruff, P. Bailey, T.C.Q. Noakes, Phys. Rev. B 61 (2000) 7706.
[29] D. Kaminski, P. Poodt, E. Aret, N. Radenovic, E. Vlieg, unpublished.
[30] R.J. Baxter, Exactly Solved Models in Statistical Mechanics, Academic Press, Inc. [Harcourt Brace Jovanovich, Publishers], London, 1982.
[31] B.M. Ocko, O.M. Magnussen, J.X. Wang, R.R. Adzic, Th. Wandlowski, Physics B 221 (1996) 238.
[32] R. Schuster, I.K. Robinson, K. Kuhnke, S. Ferrer, J. Alvarez, K. Kern, Phys. Rev. B 54 (1996) 17097.
[33] J. Frenkel, T. Kontorova, J. Phys. (USSR) 1 (1939) 137.
[34] A. Zangwill, Physics at Surfaces, Cambridge Univ. Press, Cambridge, 1988.
[35] H.L. Mayerheim, H. Zajonz, W. Moritz, I.K. Robinson, Surf. Sci. 381 (1997) L551.
[36] E. AlShamaileh, C. Barnes, Phys. Chem. Chem. Phys. 4 (2002) 5148.
[37] G. Prevot, C. Cohen, D. Schmaus, V. Pontikis, Surf. Sci. 459 (2000) 57.
[38] R. van Gastel, D. Kaminski, B. Poelsema, E. Vlieg, unpublished.